Nonradiative decay and absorption rates of quantum emitters embedded in metallic systems: Microscopic description and their determination from electronic transport

M. B. Silva Neto, F. M. D'Angelis, P. P. P. Foster, and F. A. Pinheiro
Instituto de Fisica, Universidade Federal do Rio de Janeiro, Caixa Postal 68528, Rio de Janeiro, Brazil

(Received 29 May 2018; revised manuscript received 28 September 2018; published 14 November 2018)

We investigate nonradiative decay and absorption rates of two-level quantum emitters embedded in a metal at low temperatures. We obtain the expressions for both nonradiative transition rates and identify a unique, experimentally accessible way to obtain both nonradiative transition rates via electronic transport in the host metallic system. Our findings not only provide a microscopic description of the nonradiative channels in metals, but they also allow one to identify, determine, and differentiate them from other decay channels, which is crucial to the understanding and controlling of the light-matter interactions at the nanoscale.

DOI: 10.1103/PhysRevB.98.195116

I. INTRODUCTION

Controlling and understanding light-matter interactions at the nanoscale is key for a broad range of applications, including biosensing, imaging, and quantum information processing. Among the several processes that govern light-matter interactions, spontaneous emission from quantum emitters (QE) (atoms, molecules, and quantum dots) is one of the most important for applications in nanophotonics. This radiative process strongly depends on the electromagnetic environment surrounding the QE, as discovered in the pioneering work by Purcell [1], and it has been extensively investigated in several photonic systems, such as photonic cavities [2,3], planar interfaces [4,5], photonic crystals [6,7], metamaterials [8–11], and waveguides [12,13].

In addition to the radiative relaxation, when the QE is placed near or inside metallic structures other decay pathways are available, see Fig. 1. For instance, the energy of the QE can be dissipated in a plasmonic channel, as the proximity of a QE to metal-dielectric interfaces facilitates the excitation of surface plasmon polaritons, electromagnetic excitations related to the charge density waves on the surface of the metallic structure. This mechanism leads to a strong confinement of the electromagnetic field at metal-dielectric interfaces, which is the basis of many applications to enhance light-matter interactions, such as single optical plasmon generation [14,15], single molecule detection with surface-enhanced Raman scattering [16], and nanoantenna modified spontaneous emission [17].

Nonradiative relaxation is another decay pathway, where the QE energy can be dissipated via coupling to phonons, resistive heating, or quenching by other quantum emitters. Nonradiative relaxation is particularly important in metallic systems, where emission quenching may occur due to unavoidable dissipation even in systems with high spontaneous emission rate. In many cases of practical interest increasing the ratio between radiative and nonradiative decay channels is of great importance since the former actually determines the efficiencies of photonic devices, such as LEDs [18], and single-photon sources [19]. In other situations it is very important to identify the nonradiative mechanism, distinguishing it from the plasmonic channel as it is the case of applications involving the excitation of single plasmon polaritons and subsequent controlled coupling between metallic nanowires [20,21].

In the present paper we identify a unique, experimentally accessible way to identity the nonradiative contribution to the total decay of two-level QEs inside metals. By means of a microscopic, analytical approach, we compute the nonradiative decay channel of a QE embedded in a metal, in which dissipation is due to inelastic scattering of electrons close to the Fermi surface, see Fig. 1 [22]. After computing the transition rates for both nonradiative decay and absorption, we demonstrate that such quantities can be directly determined by the knowledge of experimentally accessible transport quantities, such as the optical and ac conductivity, and even the dc resistivity. This result not only provides a microscopic description of nonradiative decay channels in metals, but also allows one to identify and differentiate it to other decay channels, which is crucial for the development of disruptive optoelectronic plasmonic applications.

There are many different physical systems of current interest in which QEs are embedded in metallic structures and hence are directly relevant to the present work. Among them one can mention: (i) Color centers in halides, oxides, and perovskites [23]. In this case, radiation-induced, anionic vacancies inside the bulk crystal can trap electrons giving rise to the so called F centers that absorb and emit light in the visible, thus being excellent candidates for solid state single photon sources. (ii) Heteroepitaxially grown, nanostructured bulk materials, such as the organohalide perovskites [24], where colloidal quantum dots (QDs) are grown inside a methylammonium lead iodide matrix (MAPbI3). Here the unique combination of the excellent electrical transport properties of the MAPbI3 matrix and the high radiative efficiency of the colloidal QDs holds promise for large-scale manufacturing of infrared optoelectronic devices, such as multijunction solar cells and blue light-emitting diodes. (iii) Defect dipoles in

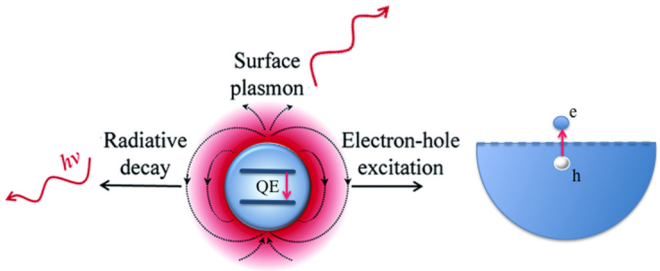

FIG. 1. Possible relaxation mechanisms for a quantum emitter (QE) bearing an electric dipole moment (thin field lines around the QE) embedded in a metal. Besides photoemission (left) and decay into surface plasmon modes (top), electric-dipole transitions in the QE can also be induced by the inelastic scattering between electronic states (electrons and holes) close to the Fermi level (right).

perovskites with the ABO_3 crystal structure, such as $PbZrO_3$, $PbTiO_3$, and $PbZr_xTi_{1-x}O_3$. These PZT systems exhibit important antiferroelectric, ferroelectric, piezoelectric, and, most importantly, photoluminescent properties [25] that make them useful in a wide range of applications such as, for example, the fabrication of dynamic random-access memory (DRAM), nonvolatile ferroelectrics random-access memory (NFRAM) devices, light emitting devices for displays and communications, piezoelectric sensors actuators and transducers, and MEMS devices. In addition to these well-known, established examples in condensed matter systems, QEs embedded in metallic systems are of increasing interest for plasmonic and metamaterials applications [26–28].

This paper is organized as follows. In Sec. II we describe the methodology to microscopically calculate the transition rates for both nonradiative decay and absorption. In Sec. III we discuss and analyze the behavior of the decay rates as a function of the temperature, whereas Sec. IV is devoted to the conclusions.

II. METHODOLOGY

The prototypical systems we consider are composed of a two-level QE, e.g., color (or F, F^-) centers, quantum dots, and dipole defects, created via irradiation, implantation, or during growth, inside bulk crystals with a robust metallic phase such as oxides, perovskites with a MAPbI3 matrix, PZT ferroelectric systems, and many others. In all such cases, an excited QE will only decay in the visible through a number of available nonradiative channels, the reason being the inability of visible light with $1.8 \leqslant \hbar\omega \leqslant 3.1$ eV to propagate as standing waves in ordinary metals, because the plasmon frequency

$$\omega_{\rm pl}^2 = \frac{e^2}{\varepsilon_0}\left(\frac{n}{m^*}\right) \tag{1}$$

is typically $\hbar\omega_{\rm pl} \sim 10$ eV. Here, as usual, e is the electric charge, ε_0 is the dielectric constant in free space, n is the electronic density in the metal, and m^* is the effective mass of the quasiparticles. In this regime, the dielectric function reads

$$\varepsilon_r(\omega) = 1 - \frac{\omega_{\rm pl}^2}{\omega^2}, \tag{2}$$

and metals are strongly absorbing for $\omega < \omega_{\rm pl}$, so that the probability of decay in a radiative channel is very small.

Nevertheless, when a QE is embedded in a metal, relaxation can still occur via the inelastic scattering of electrons close to the Fermi surface, as it is schematically illustrated on the right side of Fig. 1. In order to adequately model the coupling between the QE with the band electrons in a metal, we shall consider the following interaction Hamiltonian:

$$H = \hbar\omega_0|e\rangle\langle e| + \sum_k \epsilon_k c_k^\dagger c_k + H_{\rm int}, \tag{3}$$

where $\hbar\omega_0$ is the energy splitting between the ground $|g\rangle$ and excited $|e\rangle$ states of the two-level system, ϵ_k is the band dispersion relation for the electrons in the metal, $c_k^\dagger$ and c_k are creation and annihilation operators such that

$$\begin{aligned} c_k|FS\rangle &= \sqrt{f(\epsilon_k)}|h_k\rangle, \\ c_k^\dagger|FS\rangle &= \sqrt{1-f(\epsilon_k)}|p_k\rangle, \end{aligned} \tag{4}$$

with $|FS\rangle$ representing the Fermi sea, $|h_k\rangle$ representing the hole state, $|p_k\rangle$ representing the particle state, and with $f(\epsilon_k)$ being the Fermi-Dirac occupation probability. For simplicity we shall omit spin indices since we will be considering solely spin preserving scattering processes. The interaction part of the Hamiltonian reads

$$H_{\rm int} = \sum_{\ell,m=g,e}\sum_{k,k'} c_{k'}^\dagger c_k S(k'-k)\tilde{V}_{QD}^{\ell m}(k'-k)|\ell\rangle\langle m|, \tag{5}$$

and describes the electrostatic interaction between the electronic charge density of the electron liquid in the metal and the static impurity potential generated by the two-level system. The corresponding electric-dipole matrix element reads

$$\tilde{V}_{QD}^{\ell m}(k'-k) = -\frac{i}{V}\frac{e}{\varepsilon_0\varepsilon_{\rm TF}(k-k')}\frac{1}{|k-k'|}\hat{\xi}_{k-k'}\langle\ell|\vec{\mu}|m\rangle, \tag{6}$$

where V is the volume, $\vec{\mu}$ is the electric dipole moment of the emitter, $\hat{\xi}_{k-k'} = (k-k')/|k-k'|$ is the longitudinal unit vector along the direction of $k-k'$,

$$\varepsilon_{\rm TF}(k-k') = 1 + \frac{k_{\rm TF}^2}{|k-k'|^2} \tag{7}$$

is the Thomas-Fermi (TF) dielectric function, written in terms of the TF screening wave vector $k_{\rm TF}^2 = 3e^2n/2\varepsilon_0\epsilon_F$, for a Fermi energy ϵ_F (obtained from the standard definition of the longitudinal dielectric function). We have also introduced the impurity structure factor

$$S(k'-k) = \sum_{\mathbf{R}_i} P_{R_i} e^{i(k'-k)R_i}, \tag{8}$$

where P_{R_i} gives the probability of having an emitter at $\mathbf{R}_i$.

In what follows we shall be interested in calculating the nonradiative decay and absorption rates and, for this reason, we will restrict our calculations to the $e \to g$ and $g \to e$ processes only. For future purposes it will also be interesting to observe that the interacting part of the Hamiltonian has the general structure

$$H_{\rm int} = \sum_{k,k'} c_{k'}^\dagger c_k \tilde{V}_{QD}^{ge}(k'-k)S(k'-k)|g\rangle\langle e|. \tag{9}$$

Here $|g\rangle\langle g|$ and $|e\rangle\langle e|$ are the projection operators onto the ground $|g\rangle$ and excited $|e\rangle$ states, while $|e\rangle\langle g|$ and $|g\rangle\langle e|$ describe the electronic tunneling between the two levels. Furthermore, the eigenstates of the free Hamiltonian can be written in terms of $|\ell\rangle$ and $|FS\rangle$ as

$$|\ell; FS\rangle = |\ell\rangle \otimes |FS\rangle, \tag{10}$$

where $|\ell\rangle$ with $\ell = e, g$ are the eigenvectors of the TLS Hamiltonian, and $|FS\rangle$ are the eigenvectors of the electron Hamiltonian in the number operator representation.

III. RESULTS AND DISCUSSIONS

A. General structure for the nonradiative decay rate

In order to calculate the nonradiative decay rate we need to prepare the QE in the excited state $|e\rangle$ and then calculate the transition amplitude of decay towards the ground state $|g\rangle$ with the production of an electron-hole pair close to the Fermi level. This can be done by using Fermi's golden rule

$$\Gamma(I \to F) = \left(\frac{2\pi}{\hbar}\right)|\langle H_{IF}\rangle|^2 \delta(E_F - E_I), \tag{11}$$

with initial and final states corresponding to

$$\begin{aligned} I \equiv |e; FS\rangle &= |e\rangle \otimes |FS\rangle \to |g; h_k p_{k'}\rangle \\ &= |g\rangle \otimes |h_k p_{k'}\rangle \equiv F, \end{aligned} \tag{12}$$

where $\ell, m = g, e$, and with energies given by

$$\begin{aligned} E_I &= \hbar\omega_0, \\ E_F &= \epsilon_{k'} - \epsilon_k. \end{aligned}$$

Now the transition amplitude reads

$$\begin{aligned} \Gamma(k, k'; e, g) = \left(\frac{2\pi}{\hbar}\right) &\left|\langle F|c_{k'}^\dagger c_k \widetilde{V}_{QD}^{ge}(k' - k)|g\rangle\langle e||I\rangle\right|^2 \\ &\times \langle S(k' - k)S(k' - k)\rangle \delta(E_F - E_I), \end{aligned}$$

and can be calculated with the use of the fermionic algebra (4) and from the fact that $\langle S(k' - k)S(k' - k)\rangle = N_{\rm imp}$, for a small number of dilute impurities (emitters). We are now ready to rewrite the transition amplitude in terms of the initial and final momentum states, $|h_k\rangle$ representing the hole state, $|p_{k'}\rangle$ representing the electron state, and in terms of the occupation probabilities for the ground n_g and excited n_e states in the two-level system (see Appendix)

$$\begin{aligned} \Gamma(k, k'; e, g) = \left(\frac{2\pi}{\hbar}\right) &N_{\rm imp} f(\epsilon_k)[1 - f(\epsilon_{k'})] n_e(1 - n_g) \\ &\times \left|\widetilde{V}_{QD}^{ge}(k' - k)\right|^2 \delta(\epsilon_{k'} - \epsilon_k - \hbar\omega_0). \end{aligned} \tag{13}$$

The next step is to calculate the relaxation rates through summing up transition amplitudes

$$\Gamma_{\rm nr}^{e\to g}(T) = \sum_{k,k',\sigma,\sigma'} \Gamma(k, k'; e, g). \tag{14}$$

For the nonradiative (nr) decay from the excited to ground states we found (see Appendix)

$$\Gamma_{\rm nr}^{e\to g}(T) = \left(\frac{2\pi}{\hbar}\right) N^2(\epsilon_F) N_{\rm imp} n_e(1 - n_g)\left[\frac{1}{1 - e^{-\beta\hbar\omega_0}}\right] g_{\rm nr}^2, \tag{15}$$

where $N(\epsilon_F)$ is the electronic density of states at the Fermi level and we have defined the quantity

$$g_{\rm nr}^2 = \frac{e^2}{\varepsilon_0^2}\frac{\mu^2}{3}\frac{\hbar\omega_0}{k_F^2}\left[\frac{1}{1 + 2k_F^2\lambda_{\rm TF}^2} + \ln\left(1 + 2k_F^2\lambda_{\rm TF}^2\right) - 1\right], \tag{16}$$

in terms of the Thomas-Fermi screening length $\lambda_{\rm TF} = k_{\rm TF}^{-1}$ (see Appendix). As expected, the nonradiative decay rate vanishes at zero temperature, because there are simply no final electron-hole states available for relaxation, since $f_{T=0}(\epsilon \leqslant \epsilon_F) = 1$ and $f_{T=0}(\epsilon > \epsilon_F) = 0$. As the temperature increases, on the other hand, $f_{T\neq 0}(\epsilon \leqslant \epsilon_F) < 1$ and $f_{T\neq 0}(\epsilon > \epsilon_F) \neq 0$, and the nonradiative decay rate also increases, even for $k_B T \gg \hbar\omega_0$, when ground and excited states reach their maximal allowed values of thermal occupancy, namely $n_g(k_B T \gg \hbar\omega_0) = n_e(k_B T \gg \hbar\omega_0) = 1/2$.

B. General structure for the nonradiative absorption rate

Similarly, in order to calculate the nonradiative absorption rate we need to prepare the QE in the ground state and then calculate the transition amplitude towards the excited state through the absorption of an electron-hole pair close to the Fermi level. Now the initial and final states are

$$\begin{aligned} I \;&\equiv\; |g; h_k p_{k'}\rangle = |g\rangle \otimes |h_k p_{k'}\rangle \\ &\to |e; FS\rangle = |e\rangle \otimes |FS\rangle \equiv F. \end{aligned} \tag{17}$$

The nonradiative absorption rate is given by

$$\Gamma_{\rm nr}^{g\to e}(T) = \left(\frac{2\pi}{\hbar}\right) N^2(\epsilon_F) N_{\rm imp} n_g(1 - n_e)\left[\frac{1}{e^{\beta\hbar\omega_0} - 1}\right] g_{\rm nr}^2, \tag{18}$$

where n_e and n_g have been interchanged and the thermal factor is also different

$$\left[\frac{1}{1 - e^{-\beta\hbar\omega_0}}\right]_{\rm decay} \to \left[\frac{1}{e^{\beta\hbar\omega_0} - 1}\right]_{\rm absorption}, \tag{19}$$

satisfying detailed balance. As expected, the nonradiative absorption rate also vanishes at zero temperature, because there are no available initial electron-hole states for absorption at $T = 0$. As the temperature increases, the nonradiative absorption becomes finite, even for $k_B T \gg \hbar\omega_0$, when there are plenty of available electron-hole states for absorption and when ground and excited states reach their maximal thermal occupation.

C. Normalized decay and absorption rates

A meaningful quantity to be defined is the nonradiative decay rate normalized by its saturation value

$$\Gamma_{\rm nr}^{\rm sat}(\hbar\omega_0 \ll k_B T \ll E_F) = \left(\frac{2\pi}{\hbar}\right) N_{\rm imp}\frac{1}{4} N^2(\epsilon_F)\left(\frac{g_{\rm nr}^2}{\beta\hbar\omega_0}\right), \tag{20}$$

since, for $\hbar\omega_0 \ll k_B T \ll E_F$, $n_g \to 1/2$ and $n_e \to 1/2$. With this definition we arrive at

$$\frac{\Gamma_{\rm nr}^{e\to g}(T)}{\Gamma_{\rm nr}^{\rm sat}} = 4\, n_e(1 - n_g)\left[\frac{\beta\hbar\omega_0}{1 - e^{-\beta\hbar\omega_0}}\right], \tag{21}$$

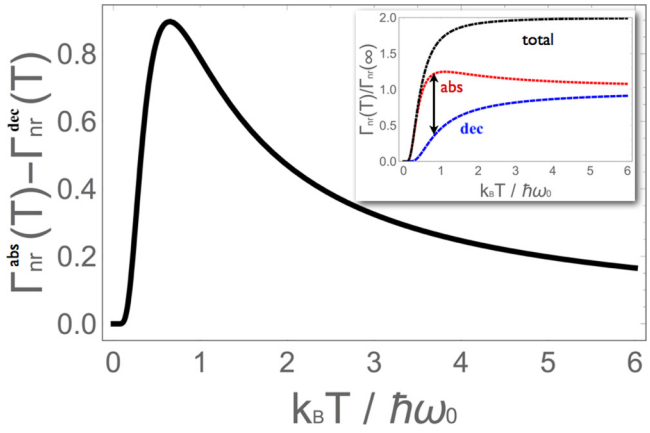

FIG. 2. Main panel: Black (solid) curve representing the relative difference between absorption and decay rates for nonradiative transitions for an emitter embedded in a low temperature metallic host. Inset: Red (dotted) curve representing the absorption rate, blue (dashed) curve representing the decay rate, and black (solid) curve representing the sum of absorption and decay rates. The curve shown in the main panel measures the distance between the red (dotted) and blue (dashed) curves in the inset.

which is a dimensionless number between 0 and 1. The same is valid for the absorption rate

$$\frac{\Gamma_{\rm nr}^{g\to e}(T)}{\Gamma_{\rm nr}^{\rm sat}} = 4\,n_g(1-n_e)\left[\frac{\beta\hbar\omega_0}{e^{\beta\hbar\omega_0}-1}\right]. \tag{22}$$

The results for both nonradiative decay and absorption rates, as well as their sum, are plotted in the inset of Fig. 2. We can also study the difference between the nonradiative absorption and decay rates

$$\Delta\Gamma_{\rm nr} \equiv \frac{\Gamma_{\rm nr}^{g\to e}(T) - \Gamma_{\rm nr}^{e\to g}(T)}{\Gamma_{\rm nr}^{\rm sat}}, \tag{23}$$

which is a quantity between 0 and 1 and is plotted as the main panel in Fig. 2.

D. A mechanism of generation

Figure 2 reveals that the absorption processes, in which a recombination of a particle and a hole provides energy for the $g \to e$ transition, dominates for $k_BT \ll \hbar\omega_0$. Absorption rapidly increases with temperature, but eventually saturates due to the decrease in the thermal occupation of the ground state for $k_BT \gg \hbar\omega_0$. On the other hand, decay processes in which a particle and a hole are created, receiving energy from the $e \to g$ transition, are less frequent at all temperatures because of the lower thermal occupation in the excited state of the emitter. Nevertheless, it also increases with the temperature and also saturates for $k_BT \gg \hbar\omega_0$.

Remarkably, let us point out that such large difference between the absorption and decay rates indicates that the phenomenon of *generation* is occurring at the emitter due to the inelastic scattering from Fermi surface states at low temperatures. This result suggests a way in which one could prepare an emitter in its excited state by setting the temperature around $k_BT \leqslant \hbar\omega_0$ where nonradiative absorption is much larger than decay. The ability to prepare quantum states of an emitter by varying the temperature is of great importance and may find many potential applications in quantum nanophotonics.

IV. CONNECTION TO ELECTRONIC TRANSPORT

Having calculated the nonradiative absorption and decay rates for QEs due to the presence of an electronic, bulk channel for quantum relaxation, one relevant question to be asked is: *how much of this nonradiative channel is relevant?* Or even better, *how could one estimate, determine, or measure* Γ_{nr} *for QEs in metals?* These are the questions we will be addressing below and consist of the main focus of the present work. Furthermore, these are very important questions to be asked if one is planning on making predictions and designing nanophotonic devices because one would like to be able to precisely determine the contribution of each decay channel to the total rate. As we are going to show below, for the case of nonradiative decay in metals the transition rates, either absorption or decay, can be precisely determined from well established and controlled transport experiments.

We shall be focused on two specific transport quantities: (i) we shall first look into the dc transport, with an externally applied electric field $E \neq 0$, where the resistivity can be expressed in a Drude-like form

$$\rho = \left(\frac{m^*}{ne^2}\right)\frac{1}{\tau_{\rm tr}}. \tag{24}$$

The quantity of interest will be the inverse transport lifetime $1/\tau_{\rm tr}$, which can be calculated using a variational approach to the linearized Boltzmann's transport equations within the relaxation time approximation [29]. (ii) Next, we shall focus on the magnetotransport, in applied electric $E \neq 0$, and magnetic $B \neq 0$ fields, where the Shubnikov–de-Haas oscillations [30,31]

$$\Delta R_{xx}(\omega_c) = 4R_0 e^{-\pi/\omega_c\tau_q}\cos\left(\frac{2\hbar\pi^2 n}{m^*\omega_c} - \pi\right)\chi(T) \tag{25}$$

are given in terms of the quantum lifetime τ_q, with R_0 being the zero field resistance, $\omega_c = eB/m^*$ the cyclotron frequency, and $\chi(T) = (2\pi^2 k_B T/\hbar\omega_c)\sinh(2\pi^2 k_B T/\hbar\omega_c)$ the thermal damping factor. The quantity of interest here is the inverse quantum lifetime $1/\tau_q$, which can also be calculated using a variational procedure [29]. For both cases (dc and magnetotransport) we shall explain how the nonradiative transition rates calculated earlier can be extracted from experiments.

A. Connection to transport lifetime $\tau_{\rm tr}$

According to the interaction Hamiltonian (5) there are four channels for scattering between the emitter and Fermi surface electrons: two elastic channels $g \to g$ and $e \to e$, and two inelastic channels $g \to e$ (absorption) and $e \to g$ (decay). The inverse transport lifetime $1/\tau_{\rm tr}$ can thus be calculated using Mathiessen's rule

$$\frac{1}{\tau_{\rm tr}} = \frac{1}{\tau_{gg}} + \frac{1}{\tau_{ge}} + \frac{1}{\tau_{eg}} + \frac{1}{\tau_{ee}}, \tag{26}$$

in which each individual contribution $1/\tau_{\ell m}$ to the total inverse scattering time can be calculated from a variational

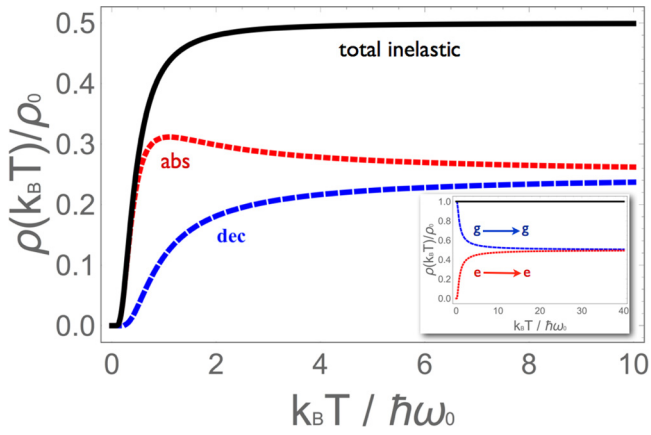

FIG. 3. Temperature dependence of the dc-resistivity $\rho(T)$, normalized by its zero temperature value ρ_0. Main panel: Inelastic channels, red (dotted) representing absorption $g \to e$, blue (dashed) representing decay $e \to g$, and black (solid) representing the sum of the two inelastic (decay and absorption) contributions. Inset: Elastic channels, red (dotted) representing $e \to e$ processes, blue (dashed) representing $g \to g$ processes, and black (solid) representing the sum of the two elastic contributions to transport.

principle to the linearized Boltzmann's equations within the relaxation time approximation [29]

$$\frac{1}{\tau_{\ell m}} = \frac{1}{2k_B T} \frac{\sum_{k,k'} [\vec{u}\cdot(\vec{v}_k - \vec{v}_{k'})]^2 P^{\ell m}_{k',k}}{\sum_k (\vec{u}\cdot\vec{v}_k)^2 \left(-\frac{\partial f_k}{\partial \epsilon_k}\right)}, \tag{27}$$

where $\vec{u}$ corresponds to the direction of the applied electric field, and $P^{\ell m}_{k',k}$ are the scattering amplitudes from $\mathbf{k}$ to $\mathbf{k}'$, between states labeled by $\ell, m = g, e$.

The denominator in (27) can be written as

$$\sum_{k,\sigma} (\vec{u}\cdot\vec{v}_k)^2 \left(-\frac{\partial f_k}{\partial \epsilon_k}\right) = \frac{1}{3\pi^2}\frac{v_F}{\hbar} = \frac{n}{m^*}, \tag{28}$$

where the factor $1/3$ arises from the spherical symmetry of the problem. As for the numerator in (27) we shall write

$$\langle P^{\ell m}\rangle_{tr} = \frac{1}{2k_B T} \sum_{k,k'} [\vec{u}\cdot(\vec{v}_k - \vec{v}_{k'})]^2 P^{\ell m}_{k',k}, \tag{29}$$

where the scattering amplitudes are given in the Appendix. For the two elastic scattering processes we find

$$\langle P^{gg}\rangle_{\rm tr} = \left(\frac{2\pi}{\hbar}\right) N^2(\epsilon_F) N_{\rm imp} n_g g^2_{\rm el} \tag{30}$$

and

$$\langle P^{ee}\rangle_{\rm tr} = \left(\frac{2\pi}{\hbar}\right) N^2(\epsilon_F) N_{\rm imp} n_e g^2_{\rm el}, \tag{31}$$

where

$$g^2_{\rm el} = \frac{1}{6}\frac{e^2}{\varepsilon_0^2}\left(\frac{\hbar}{m^*}\right)^2 \frac{1}{k_F^2}\left[\frac{1}{1+2k_F^2\lambda^2_{\rm TF}} + \ln\left(1+2k_F^2\lambda^2_{\rm TF}\right) - 1\right]. \tag{32}$$

The elastic contributions to the resistivity are shown in the inset of Fig. 3. As we can see, the sum of the two elastic contributions is temperature independent mostly because

TABLE I. Summary of the results for the nonradiative transition rates and their relation to the quantum and transport lifetimes obtained from transport. Notice the one-to-one relation between the NR rates and the quantum lifetimes $1/\tau_q$, and the proportionality relation to the transport lifetimes $1/\tau_{\rm tr}$, a direct consequence of the suppression of small angle scattering in the calculation of the Boltzmann transport lifetime resulting in the factor $(g^2_{\rm nr}/g^2_{\rm in}) < 1$.

Nonradiative rates	Quantum lifetimes	Transport lifetimes
Decay $\Gamma^{e\to g}_{\rm nr}$	$1/\tau_q^{e\to g}$	$1/\tau_{\rm tr}^{e\to g}\left(g^2_{\rm nr}/g^2_{\rm in}\right)$
Absorption $\Gamma^{g\to e}_{\rm nr}$	$1/\tau_q^{g\to e}$	$1/\tau_{\rm tr}^{g\to e}\left(g^2_{\rm nr}/g^2_{\rm in}\right)$

$n_g + n_e = 1$ and $\tilde{V}^{gg} = \tilde{V}^{ee}$, even though each of the two individual scattering channels exhibits a characteristic evolution with the temperature until saturation at $n_e = n_g = 1/2$ for $k_B T \gg \hbar\omega_0$. Furthermore, since this contribution has its origins in elastic processes, $1/\tau_{gg}$ and $1/\tau_{ee}$ do not contain information about the structure of the emitter, neither through the electric dipole moment $\vec{\mu}$, nor through the characteristic energy of the emitter $\hbar\omega_0$. Hence the elastic contributions to the resistivity have no connection to the transition rates calculated earlier.

For the two inelastic scattering processes, in turn, we have

$$\langle P^{ge}\rangle_{\rm tr} = \left(\frac{2\pi}{\hbar}\right) N^2(\epsilon_F) N_{\rm imp} n_g (1-n_e)\left[\frac{\beta}{e^{\beta\hbar\omega_0}-1}\right] g^2_{\rm in} \tag{33}$$

and

$$\langle P^{eg}\rangle_{\rm tr} = \left(\frac{2\pi}{\hbar}\right) N^2(\epsilon_F) N_{\rm imp} n_e (1-n_g)\left[\frac{\beta}{1-e^{-\beta\hbar\omega_0}}\right] g^2_{\rm in}, \tag{34}$$

where

$$g^2_{\rm in} = \frac{e^2}{\varepsilon_0^2}\frac{\mu^2}{3}\frac{\hbar\omega_0}{\lambda^2_{\rm TF}}\left(\frac{\hbar}{m^*}\right)^2 \times \left[\frac{2k_F^2\lambda^2_{\rm TF}\left(1+k_F^2\lambda^2_{\rm TF}\right)}{1+2k_F^2\lambda^2_{\rm TF}} - \ln\left(1+2k_F^2\lambda^2_{\rm TF}\right)\right]. \tag{35}$$

The inelastic contributions to the resistivity are shown in the main panel of Fig. 3. In contrast to the elastic case, both the individual contributions to the resistivity, as well as their sum, have a strong temperature dependence that is analogous to the temperature dependence of the normalized decay and absorption rates shown in Fig. 2.

Also differently to the elastic case, the inelastic contributions $1/\tau_{eg}$ and $1/\tau_{ge}$ do carry information about the structure of the emitter, through both the electric dipole moment $\vec{\mu}$ and the characteristic energy $\hbar\omega_0$. Indeed, it is important to note the direct connection that exists between the nonradiative decay rate, given by (15), and the inelastic scattering process given by (34). Both quantities are proportional to $\mu^2\hbar\omega_0$ and only differ by an overall constant factor, see $g^2_{\rm nr}$ in (16) and $g^2_{\rm in}$ in (35) (see Table I). By the same token, a similar mapping exists between the nonradiative absorption rate (18) and the other inelastic scattering process, given by (33). Again, these two quantities only differ by a constant factor (see Table I). Altogether, these findings unveil the relation between nonradiative decay and absorption rates and the inelastic scattering

processes that are summarized in Table I, suggesting that one can obtain information about nonradiative decay and absorption rates by means of electronic transport.

B. Connection to quantum lifetime τ_q

Similar to the case of the dc resistivity, the quantum lifetime can also be calculated, using Mathiessen's rule

$$\frac{1}{\tau_q} = \frac{1}{\tau_{gg}} + \frac{1}{\tau_{ge}} + \frac{1}{\tau_{eg}} + \frac{1}{\tau_{ee}}, \tag{36}$$

where now each contribution corresponds to [29]

$$\frac{1}{\tau_{\ell m}} = \frac{1}{k_B T} \frac{\sum_{k,k'} P^{\ell m}_{k',k}}{\sum_k \left(-\frac{\partial f_k}{\partial \epsilon_k}\right)}. \tag{37}$$

Again, for the numerator in (37) we define

$$\langle P^{\ell m} \rangle_q = \frac{1}{k_B T} \sum_{k,k'} P^{\ell m}_{k',k}. \tag{38}$$

For the two inelastic scattering processes we obtain

$$\langle P^{ge} \rangle_q = \left(\frac{2\pi}{\hbar}\right) N^2(\epsilon_F) N_{\rm imp} n_g (1 - n_e) \left[\frac{\beta}{e^{\beta\hbar\omega_0} - 1}\right] g^2_{\rm nr} \tag{39}$$

and

$$\langle P^{eg} \rangle_q = \left(\frac{2\pi}{\hbar}\right) N^2(\epsilon_F) N_{\rm imp} n_e (1 - n_g) \left[\frac{\beta}{1 - e^{-\beta\hbar\omega_0}}\right] g^2_{\rm nr}, \tag{40}$$

where

$$g^2_{\rm nr} = \frac{e^2}{\varepsilon_0^2} \frac{\mu^2}{3} \frac{\hbar\omega_0}{k_F^2} \left[\frac{1}{1 + 2k_F^2 \lambda^2_{\rm TF}} + \ln\left(1 + 2k_F^2 \lambda^2_{\rm TF}\right) - 1\right]. \tag{41}$$

Remarkably, we now obtain that for the quantum lifetime $1/\tau_q$ there exists a one-to-one correspondence between the nonradiative decay and absorption rates $\Gamma^{e\to g}_{\rm nr}$ and $\Gamma^{g\to e}_{\rm nr}$, and the inelastic contributions to electron-impurity scattering processes $1/\tau_{eg}$ and $1/\tau_{ge}$ (see Table I). These results confirm our predictions that one can determine the nonradiative decay and absorption rates by means of magnetotransport observables such as, for example, the amplitude of the Shubnikov–de-Haas oscillations which is given by [32]

$$\Delta R(\omega_c) = 4 R_0 \chi(T)\, e^{-\pi/\omega_c \tau_q}, \tag{42}$$

which is governed by τ_q and it is shown in the main panel of Fig. 4. From such a Dingle plot [32] we see that, already at small magnetic fields, $\omega_0/\omega_c \gg 1$, even the smallest contributions to the quantum lifetime τ_q from nonradiative transitions may lead to sizable deviations of the amplitude of the Shubnikov–de-Haas oscillations from the pure elastic case at $k_B T \ll \hbar\omega_0$. If we recall that for $k_B T \leqslant \omega_0$ absorption processes dominate, as demonstrated in Fig. 2, we can promptly identify that the deviation of the dashed (blue) curve from the solid (black) curve in Fig. 4 is predominantly due to absorption processes $\Gamma^{g\to e}_{\rm nr} \gg \Gamma^{e\to g}_{\rm nr}$. On the other hand, for the dotted (red) curve in Fig. 4, valid for $k_B T \gg \hbar\omega_0$, both decay and absorption processes contribute equally, so that $\Gamma^{g\to e}_{\rm nr} \approx \Gamma^{e\to g}_{\rm nr}$. These findings suggest one cannot only extract nonradiative decay rates from the Shubnikov–de-Haas oscillations via the quantum lifetime, but also detect the presence of the emitters inside a metallic system, as nonradiative decay rates strongly depend on temperature, as we previously demonstrate.

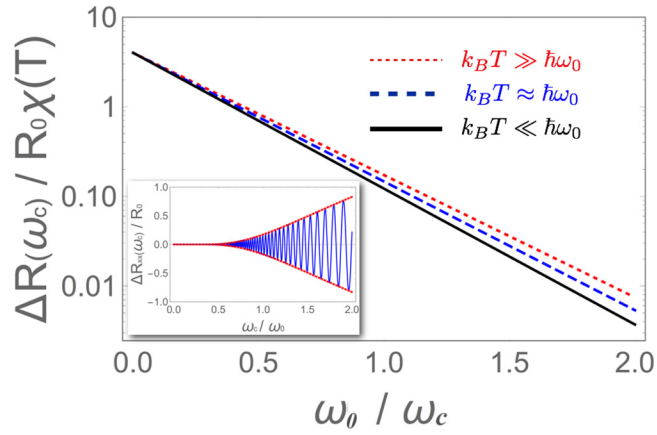

FIG. 4. Main panel: Amplitude of the Shubnikov–de-Haas oscillations for the case of $\omega_0 < \omega_c$ for different temperatures. Solid (black) line for $k_B T \ll \hbar\omega_0$; dashed (blue) line for $k_B T \approx \hbar\omega_0$; and dotted (red) line for $k_B T \gg \hbar\omega_0$. Inset: Shubnikov–de-Haas oscillations at low magnetic fields, for the case of $\omega_c < \omega_0$.

V. CONCLUSIONS

In summary, we investigate nonradiative decay and absorption rates of two-level quantum emitters embedded in a metal at low temperatures. Using Fermi's golden rule, we derive expressions for both nonradiative transition rates, showing they are intrinsically related to electronic transport in the host metallic material. Indeed, we demonstrate nonradiative decay and absorption rates could be directly determined by the knowledge of experimentally accessible transport quantities, such as the optical and ac conductivity, and even the dc resistivity. For concreteness, we consider the case of Shubnikov–de-Haas oscillations, governed by the quantum lifetime, which we demonstrate to be proportional to the nonradiative decay and absorption rates. Altogether our results not only provide a microscopic description of nonradiative decay channels in metals, but they also allows one to identify and differentiate them to other decay channels, which is crucial to understand and control light-matter interactions at the nanoscale.

ACKNOWLEDGMENTS

We thank F. S. S. Rosa, C. Farina, and L. S. Menezes for fruitful discussions. We acknowledge CNPq, CAPES, and FAPERJ for financial support. F.A.P. also thanks the The Royal Society-Newton Advanced Fellowship (Grant No. NA150208) for financial support.

APPENDIX

1. Occupation probabilities two-level system

The two occupation probabilities $n_g(k_B T)$ and $n_e(k_B T)$ can be determined from the statistical definition

$$n_i = \frac{\exp(-\beta\varepsilon_i)}{Z}, \tag{A1}$$

where

$$Z = \sum_{i=\text{all-states}} \exp(-\beta\varepsilon_i) \tag{A2}$$

is the partition function of the two-level system. From this definition we obtain

$$n_g(k_BT) = \frac{\exp(-\beta\varepsilon_g)}{\exp(-\beta\varepsilon_g)+\exp(-\beta\varepsilon_e)} = \frac{1}{1+\exp(-\beta\hbar\omega_0)} \tag{A3}$$

and

$$n_e(k_BT) = \frac{\exp(-\beta\varepsilon_e)}{\exp(-\beta\varepsilon_g)+\exp(-\beta\varepsilon_e)} = \frac{1}{1+\exp(\beta\hbar\omega_0)}. \tag{A4}$$

As it is expected, at low temperatures we have

$$\lim_{T\longrightarrow 0} n_g(k_BT) \longrightarrow 1 \tag{A5}$$

and

$$\lim_{T\longrightarrow 0} n_e(k_BT) \longrightarrow 0, \tag{A6}$$

while at large temperatures

$$\lim_{T\longrightarrow \infty} n_g(k_BT) \longrightarrow \tfrac{1}{2} \tag{A7}$$

and

$$\lim_{T\longrightarrow \infty} n_e(k_BT) \longrightarrow \tfrac{1}{2}. \tag{A8}$$

2. Calculation of decay and absorption transition rates

To sum over transition amplitudes we use the relation

$$\sum_{k,\sigma} \to V \times 2 \times \int \frac{d\epsilon_k}{\hbar v_k} \int \frac{d\Omega_k}{(2\pi)^3}, \tag{A9}$$

where the factor 2 accounts for spin degeneracy, $v_k = \hbar k/m^*$ is the velocity for a nearly free electron, parabolic band approximation with effective mass m^*, and

$$d\Omega_k = k^2 d\Omega = k^2 \sin\varphi d\theta d\varphi. \tag{A10}$$

The nonradiative (nr) decay from the excited to ground states is then calculated as

$$\begin{aligned}
\Gamma_{\text{nr}}^{e\to g}(T) &= \sum_{k,k',\sigma,\sigma'} \Gamma(k,k';e,g) \\
&= V^2 \times 4 \times \left(\frac{2\pi}{\hbar}\right) N_{\text{imp}} n_e(1-n_g) \\
&\quad \times \left\{ \int \frac{d\epsilon_k}{\hbar v_k} \int \frac{d\epsilon_{k'}}{\hbar v_{k'}} f(\epsilon_k)[1-f(\epsilon_{k'})] \right\} \\
&\quad \times \left\{ \int \frac{d\Omega_k}{(2\pi)^3} \int \frac{d\Omega_{k'}}{(2\pi)^3} \left|\widetilde{V}_{QD}^{ge}(k'-k)\right|^2 \right\} \\
&= \left(\frac{2\pi}{\hbar}\right)\left(\frac{m^*k_F}{\pi^2\hbar^2}\right)^2 N_{\text{imp}} n_e(1-n_g)\left[\frac{\hbar\omega_0}{1-e^{-\beta\hbar\omega_0}}\right] \\
&\quad \times \frac{e^2}{\varepsilon_0^2}\frac{\mu^2}{3}\left[\int \frac{d\Omega}{4\pi}\int \frac{d\Omega'}{4\pi} \frac{|k-k'|^2}{\left(|k-k'|^2+\lambda_{\text{TF}}^{-2}\right)^2}\right],
\end{aligned}$$

and we identify the electronic density of states at the Fermi level

$$N(\epsilon_F) = \frac{m^*k_F}{\pi^2\hbar^2}. \tag{A11}$$

To arrive at the above result we have used that, at low temperatures, the function

$$f(\epsilon_k)[1-f(\epsilon_k+\hbar\omega_0)] \tag{A12}$$

is strongly peaked around the Fermi energy and thus we projected all states $k \to k_F$ and $k' \to k_F$. Furthermore, we calculated

$$\int d\epsilon_k f(\epsilon_k)[1-f(\epsilon_k+\hbar\omega_0)] = \frac{\hbar\omega_0}{1-e^{-\beta\hbar\omega_0}}. \tag{A13}$$

3. Transport and quantum scattering amplitudes

The scattering amplitudes contributing to both the transport τ_{tr} and quantum τ_q lifetimes are

$$P_{k',k}^{gg} = \left(\frac{2\pi}{\hbar}\right) N_{\text{imp}} \left|\widetilde{V}_{QD}^{gg}(k'-k)\right|^2 \delta(\epsilon_k-\epsilon_{k'}) f_k(1-f_{k'}) n_g, \tag{A14}$$

$$\begin{aligned}
P_{k',k}^{eg} &= \left(\frac{2\pi}{\hbar}\right) N_{\text{imp}} \left|\widetilde{V}_{QD}^{eg}(k'-k)\right|^2 \delta(\epsilon_k-\epsilon_{k'}-\hbar\omega_0) \\
&\quad \times f_k(1-f_{k'}) n_g(1-n_e),
\end{aligned} \tag{A15}$$

$$\begin{aligned}
P_{k',k}^{ge} &= \left(\frac{2\pi}{\hbar}\right) N_{\text{imp}} \left|\widetilde{V}_{QD}^{ge}(k'-k)\right|^2 \delta(\epsilon_{k'}-\epsilon_k-\hbar\omega_0) \\
&\quad \times f_k(1-f_{k'}) n_e(1-n_g),
\end{aligned} \tag{A16}$$

$$P_{k',k}^{ee} = \left(\frac{2\pi}{\hbar}\right) N_{\text{imp}} \left|\widetilde{V}_{QD}^{ee}(k'-k)\right|^2 \delta(\epsilon_k-\epsilon_{k'}) f_k(1-f_{k'}) n_e. \tag{A17}$$

a. Transport lifetime

For the calculation of the transport lifetime τ_{tr}, the two elastic scattering processes give

$$\begin{aligned}
\langle P^{gg}\rangle_{\text{tr}} &= \frac{4V^2}{2k_BT}\int \frac{d^3k'}{(2\pi)^3}\int \frac{d^3k}{(2\pi)^3}[\vec{u}\cdot(\vec{v}_k-\vec{v}_{k'})]^2 P_{k,k'}^{gg} \\
&= \left(\frac{2\pi}{\hbar}\right) N^2(\epsilon_F) N_{\text{imp}} n_g g_{\text{el}}^2
\end{aligned} \tag{A18}$$

and

$$\begin{aligned}
\langle P^{ee}\rangle_{\text{tr}} &= \frac{4V^2}{2k_BT}\int \frac{d^3k'}{(2\pi)^3}\int \frac{d^3k}{(2\pi)^3}[\vec{u}\cdot(\vec{v}_k-\vec{v}_{k'})]^2 P_{k,k'}^{ee} \\
&= \left(\frac{2\pi}{\hbar}\right) N^2(\epsilon_F) N_{\text{imp}} n_e g_{\text{el}}^2,
\end{aligned} \tag{A19}$$

where

$$g_{\text{el}}^2 = \frac{1}{6}\frac{e^2}{\varepsilon_0^2}\left(\frac{\hbar}{m^*}\right)^2 \frac{1}{k_F^2}\left[\frac{1}{1+2k_F^2\lambda_{\text{TF}}^2} + \ln\left(1+2k_F^2\lambda_{\text{TF}}^2\right) - 1\right]. \tag{A20}$$

For the two inelastic scattering processes we have

$$\langle P^{ge}\rangle_{\rm tr} = \frac{4V^2}{2k_BT}\int\frac{d^3k'}{(2\pi)^3}\int\frac{d^3k}{(2\pi)^3}[\vec{u}\cdot(\vec{v}_k-\vec{v}_{k'})]^2P^{ge}_{k,k'} = \left(\frac{2\pi}{\hbar}\right)N^2(\epsilon_F)N_{\rm imp}n_g(1-n_e)\left[\frac{\beta}{e^{\beta\hbar\omega_0}-1}\right]g^2_{\rm in} \tag{A21}$$

and

$$\langle P^{eg}\rangle_{\rm tr} = \frac{4V^2}{2k_BT}\int\frac{d^3k'}{(2\pi)^3}\int\frac{d^3k}{(2\pi)^3}[\vec{u}\cdot(\vec{v}_k-\vec{v}_{k'})]^2P^{eg}_{k,k'} = \left(\frac{2\pi}{\hbar}\right)N^2(\epsilon_F)N_{\rm imp}n_e(1-n_g)\left[\frac{\beta}{1-e^{-\beta\hbar\omega_0}}\right]g^2_{\rm in}, \tag{A22}$$

where

$$g^2_{\rm in} = \frac{e^2}{\varepsilon_0^2}\frac{\mu^2}{3}\frac{\hbar\omega_0}{\lambda^2_{\rm TF}}\left(\frac{\hbar}{m^*}\right)^2 \times\left[\frac{2k_F^2\lambda^2_{\rm TF}\left(1+k_F^2\lambda^2_{\rm TF}\right)}{1+2k_F^2\lambda^2_{\rm TF}}-\ln\left(1+2k_F^2\lambda^2_{\rm TF}\right)\right]. \tag{A23}$$

b. Quantum lifetime

Similarly, for the case of the quantum lifetime τ_q, the two contributing inelastic scattering processes are calculated as

$$\langle P^{ge}\rangle_{q} = \frac{4V^2}{k_BT}\int\frac{d^3k'}{(2\pi)^3}\int\frac{d^3k}{(2\pi)^3}P^{ge}_{k,k'} = \left(\frac{2\pi}{\hbar}\right)N^2(\epsilon_F)N_{\rm imp}n_g(1-n_e)\left[\frac{\beta}{e^{\beta\hbar\omega_0}-1}\right]g^2_{\rm nr} \tag{A24}$$

and

$$\langle P^{eg}\rangle_{q} = \frac{4V^2}{k_BT}\int\frac{d^3k'}{(2\pi)^3}\int\frac{d^3k}{(2\pi)^3}P^{eg}_{k,k'} = \left(\frac{2\pi}{\hbar}\right)N^2(\epsilon_F)N_{\rm imp}n_e(1-n_g)\left[\frac{\beta}{1-e^{-\beta\hbar\omega_0}}\right]g^2_{\rm nr}, \tag{A25}$$

where

$$g^2_{\rm nr} = \frac{e^2}{\varepsilon_0^2}\frac{\mu^2}{3}\frac{\hbar\omega_0}{k_F^2}\left[\frac{1}{1+2k_F^2\lambda^2_{\rm TF}}+\ln\left(1+2k_F^2\lambda^2_{\rm TF}\right)-1\right]. \tag{A26}$$

[1] E. M. Purcell, Phys. Rev. **69**, 681 (1946).
[2] G. Björk, S. Machida, Y. Yamamoto, and K. Igeta, Phys. Rev. A **44**, 669 (1991).
[3] J. M. Gérard, B. Sermage, B. Gayral, B. Legrand, E. Costard, and V. Thierry-Mieg, Phys. Rev. Lett. **81**, 1110 (1998).
[4] H. P. Urbach and G. L. J. A. Rikken, Phys. Rev. A **57**, 3913 (1998).
[5] J. Johansen, S. Stobbe, I. S. Nikolaev, T. Lund-Hansen, P. T. Kristensen, J. M. Hvam, W. L. Vos, and P. Lodahl, Phys. Rev. B **77**, 073303 (2008).
[6] E. Yablonovitch, Phys. Rev. Lett. **58**, 2059 (1987).
[7] P. Lodahl, A. F. van Driel, I. S. Nikolaev, A. Irman, K. Overgaag, D. Vanmaekelbergh, and W. L. Vos, Nature (London) **430**, 654 (2004).
[8] V. V. Klimov, Opt. Commun. **211**, 183 (2002).
[9] C. L. Cortes, W. Newman, S. Molesky, and Z. Jacob, J. Opt. **14**, 063001 (2012).
[10] Z. Jacob, I. I. Smolyaninov, and E. E. Narimanov, Appl. Phys. Lett. **100**, 181105 (2012).
[11] W. J. M. Kort-Kamp, F. S. S. Rosa, F. A. Pinheiro, and C. Farina, Phys. Rev. A **87**, 023837 (2013).
[12] Y. Chen, T. R. Nielsen, N. Gregersen, P. Lodahl, and J. Mork, Phys. Rev. B **81**, 125431 (2010).
[13] S. Kumar, A. Huck, and U. L. Andersen, Nano Lett. **13**, 1221 (2013).
[14] A. V. Akimov, A. Mukherjee, C. L. Yu, D. E. Chang, A. S. Zibrov, P. R. Hemmer, H. Park, and M. D. Lukin, Nature (London) **450**, 402 (2007).
[15] D. E. Chang, A. S. Sorensen, P. R. Hemmer, and M. D. Lukin, Phys. Rev. Lett. **97**, 053002 (2006).
[16] S. Nie and S. R. Emory, Science **275**, 1102 (1997).
[17] T. H. Taminiau, F. D. Stefani, F. B. Segerink, and N. F. van Hulst, Nat. Photon. **2**, 234 (2008).
[18] S. Fan, P. R. Villeneuve, J. D. Joannopoulos, and E. F. Schubert, Phys. Rev. Lett. **78**, 3294 (1997).
[19] M. D. Eisaman, J. Fan, A. Migdall, and S. V. Polyakov, Rev. Sci. Instrum. **82**, 071101 (2011).
[20] S. Kumar, N. I. Kristiansen, A. Huck, and U. L. Andersen, Nano Lett. **14**, 663 (2014).
[21] A. Pors and S. I. Bozhevolnyi, ACS Photon. **2**, 228 (2015).
[22] M. Valenti, M. P. Jonsson, G. Biskos, A. Schmidt-Ott, and W. A. Smith, J. Mater. Chem. A **4**, 17891 (2016).
[23] E. A. Kotomin and A. I. Popov, Nucl. Instrum. Methods Phys. Res. **141** 1 (1998); J. H. Schulman and W. D. Compton, *Color Centers in Solids* (Macmillan, New York, 1962).
[24] Z. Ning, X. Gong, R. Comin, G. Walters, F. Fan, O. Voznyy, E. Yassitepe, A. Buin, S. Hoogland, and E. H. Sargent, Nature (London) **523**, 324 (2015).
[25] M. S. Silva *et al.*, J. Lumin. **111**, 205 (2005); M. Anicete-Santos *et al.*, *ibid.* **127**, 689 (2007).
[26] M. Hensen, T. Heilpern, and S. K. Gray, W. Pfeiffer, ACS Photon. **5**, 240 (2018).
[27] R. Chikkaraddy, B. de Nijs, F. Benz, S. J. Barrow, O. A. Scherman, E. Rosta, A. Demetriadou, P. Fox, O. Hess, and J. Baumberg, Nature (London) **535**, 127 (2016).
[28] D. J. Roth, A. V. Krasavin, A. Wade, W. Dickson, A. Murphy, S. Kéna-Cohen, R. Pollard, G. A. Wurtz, D. Richards, S. A. Maier, and A. V. Zayats, ACS Photon. **4**, 2513 (2017).
[29] P. B. Allen, in *Quantum Theory of Real Materials*, edited by J. R. Chellkowsky and S. G. Loule (Kluwer, Boston, 1996), Chap. 17, pp. 219–250.
[30] L. Shubnikov and W. de Haas, Leiden Commun. **207a**, 3 (1930); **207c**, 17 (1930); **207d**, 35 (1930); **210a**, 3 (1930).
[31] A. Isihara and L. Smrcka, J. Phys. C **19**, 6777 (1986).
[32] P. T. Coleridge, R. Stoner, and R. Fletcher, Phys. Rev. B **39**, 1120 (1989); P. T. Coleridge, *ibid.* **44**, 3793 (1991).